

## Flexural behavior of porous functionally graded plates using a novel higher order theory

B. Sidda Reddy<sup>a,\*</sup> and K. Vijaya Kumar Reddy<sup>b</sup>

<sup>a</sup> Rajeev Gandhi Memorial College of Engineering & Technology, Nandyal., Kurnool, A.P, India

<sup>b</sup> Jawaharlal Nehru Technological Univeristy, Hyderabad, Telangana, India

### ARTICLE INFO

#### Article history:

Received: 27 February 2020

Accepted: 4 March 2020

#### Keywords:

Functionally graded plates

Porosities

Flexure

Rule of Mixtures

Navier's method

### ABSTRACT

In this paper, the flexural response of functionally graded plates with porosities is investigated using a novel higher order shear deformation theory, which considers the influence of thickness stretching. This theory fulfills the nullity conditions at the top and bottom of the plate for the transverse shear stresses, thus avoids the need of a shear correction factor. The effective material properties are computed through the rule of mixtures. The principle of virtual displacements is employed to derive the equilibrium equations. The Navier's method is adopted to obtain the solutions in closed form for simply supported boundary conditions. The accuracy and consistency of the developed theory are established with numerical results of perfect and porous functionally graded plates available in the open literature. The dimensionless transverse displacements and stresses have been reported. The effect of even, uneven and logarithmically-uneven porosity distributions with different porosity volume fraction, gradation index, side-to thickness ratios and aspect ratios are studied. The numerical results show that, the increase of volume fraction of porosity increases the dimensionless transverse deflections and axial stresses, and decreases the transverse shear stresses. No variation of transverse shear stresses observed for a completely ceramic and metallic plate for all kinds of porosity models. The provided numerical results can be used to evaluate various plate theories and also to compare the results of other analytical methods and finite element methods.

### 1. Introduction

The combined materials usage is increasing gradually due to the inability of conventional engineering materials to meet the desired properties needed by the aerospace and many of other industries. The desired properties for aircraft, space vehicles, shipbuilding, automotive, civil, chemical, biomedical, energy sources, optical and mechanical engineering applications, can be achieved by employing the functionally graded materials (FGMs). These desired properties are attained by grading the physical properties in the thickness/length direction from one side to another side of the plate. However, in the sintering process while producing FGMs, micro voids and porosities may occur in the material. This is owing to the metal phase coagulated at very high temperature and ceramic phase is at a relatively low temperature. The presence of pores will exotically weaken the strength of the material [1]. So, it is essential to study the porosity effect in designing the FGM components. The plates are the key elements in structural systems made of FGMs. So, it is important to

investigate the flexural response of functionally graded plates (FGPs) with distributed porosities.

In the last few decades, the investigators contributed a lot in investigating the mechanical behavior of perfect FGPs without considering the porosity. The open literature reveals that, many researchers have paid their attention to discuss the vibration and buckling responses of FGPs with porosities. A nice literature review of the above mentioned works may be found in the papers of Zenkour [8] and Merdaci [11]. Mohammadi et al. [2] analyzed the vibration of thin sector plates resting on a Pasternak elastic foundation with different sector angles and elastic parameters using the new version of the differential quadrature method. Mohammadi et al [3], also investigated the circular and annular graphene sheet embedded in a Visco-Pasternak foundation under vibration by coupling with the temperature change and under in-plane pre-load. Safarabadi et al. [4] studied the surface effects on the vibration behavior of rotating nanobeam by Gurtin-Murdoch model. Baghani et al. [5] studied the dynamic and stability

\* Corresponding author. Tel.: +91-9440-844-0600; fax: +91-851-427-5123; e-mail: [bsrrgmct@gmail.com](mailto:bsrrgmct@gmail.com)

behavior of nano-beam under the effect of magnetic field, surface energy and compressive axial load using the nonlocal elasticity theory and the Gurtin Murdoch model. Goodarzi et al. [6], investigated the vibration analysis of FG circular and annular nano-plate embedded in a Visco-Pasternak foundation by varying the temperature.

Akbas [7] investigated the influence of porosity and gradation index on the free vibration and bending behavior of FGPs with all sides are simply supported (S-S-S-S). The flexural behavior of FGPs with single layer and sandwich plate with porosities was investigated by Zenkour [8]. Nguyen et al. [9], studied the nonlinear response of FG plates using  $C^0$  type higher order theory. The bending, buckling and natural frequency analyses of nano FG porous plates buildup with graphene platelets were investigated by Li et al. [10]. Merdaci [11] analyzed the flexural response of rectangular FG plates with porosities by a higher order theory with four unknowns. Demirhan and Taskin [12] used state-space approach to provide benchmark results for bending and free vibration of FG rectangular plates with porosity. In this paper the inplane and transverse displacements are separated into bending & shear components.

Kim et al. [13-14] presented the numerical results for bending, vibration & buckling of FG porous micro plates. These plate theories were not satisfied the nullity conditions. The effect of porosity, exponent index and length scale factor of the material were examined. Yang et al. [15] compared the bending and the buckling response of different form of porous FG plates with a traditional sandwich plate. The solutions were obtained by using Ritz method in combination with Chebyshev polynomials. The bending behavior of functionally graded sandwich plates with even, uneven, logarithmically uneven and linear-uneven porosities were investigated by Daikh et al. [16]. Merdaci and Belghoul [17] investigated the deflections and stresses in FG porous plates using sinusoidal shear deformation theory. The authors considered the even distribution of porosity in FG plate. Amir Farzam and Behrooz Hassani [18] analyzed the static response of FG micro plates with porosities by employing Isogeometric analysis and modified couple stress theory.

In this paper, an analytical solution is developed to investigate the flexural behavior of porous FGPs using a hyperbolic trigonometric quasi 3-D higher order theory with different forms of porosities considering the transverse extensibility in the thickness direction. The present theory uses the novel shear strain function that assesses the boundary conditions without restrictions on the top and bottom of the FGPs, thus avoids the need of a shear correction factor. The physical properties across the thickness of the FG porous plates are assumed to vary according to a power law while the Poisson's ratio keeps on constant. Navier solution is obtained in closed form for simply supported FGPs subjected to bi-sinusoidal load. The numerical results are compared with 3-D exact solutions and with other higher order theories. The influence of thickness ratios, aspect ratios, gradation index, and porosity distribution and also the volume fraction of porosity on the displacements and stresses are discussed in detail.

**2. Problem formulation**

Figure 1 represents a FG plate with physical dimensions, which contains the ceramic material at the top and the metallic material at the bottom. The FG plate also has porosities, which can be distributed evenly, unevenly or logarithmically-uneven through the plate thickness.

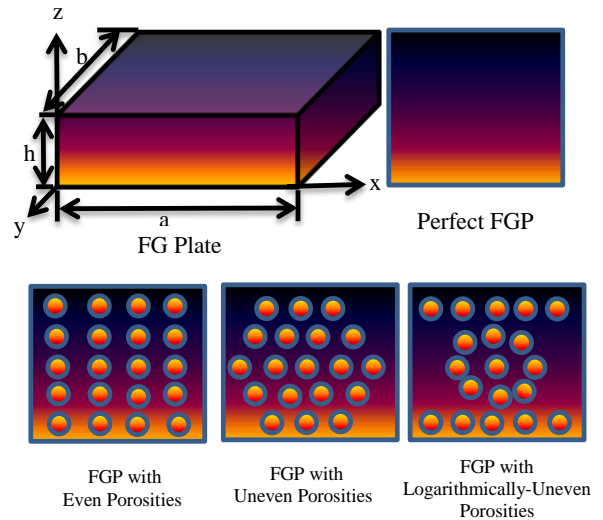


**Figure.1.** FG plate with three types of porosity distributions

The FG plate is subjected to bi-sinusoidal load  $q(x, y)$ . The effective physical properties in the thickness direction of the FG plates for three kinds of porosity distributions within the ceramic and metal phases can be given as [19]

**Even porosity model:**

$$P(z) = (P_t - P_b) \left(\frac{z}{h} + \frac{1}{2}\right)^p + P_b - \frac{\zeta}{2}(P_t + P_b) \tag{1a}$$

**Uneven porosity model:**

$$P(z) = (P_t - P_b) \left(\frac{z}{h} + \frac{1}{2}\right)^p + P_b - \frac{\zeta}{2}(P_t + P_b) \left(1 - \frac{2|z|}{h}\right) \tag{1b}$$

**Logarithmically-uneven porosity model**

$$P(z) = (P_t - P_b) \left(\frac{z}{h} + \frac{1}{2}\right)^p + P_b - \text{Log} \left(1 + \frac{\zeta}{2}\right) (P_t + P_b) \left(1 - \frac{2|z|}{h}\right) \tag{1c}$$

Where,  $P_t, P_b$  are the properties at the top and bottom of the plate respectively, including the modulus of elasticity, poisons ratio and density,  $p$  is the gradation index, thickness is  $h$  and  $\zeta$  is the volume fraction of porosity.  $\zeta = 0$  represents the perfect FG plate.

Figure 2 depicts the variation of effective Young's Modulus of Al/Al<sub>2</sub>O<sub>3</sub> perfect and FG plates with three types of porosity models. In this, the effective modulus of elasticity is assessed using the rule of mixtures with volume fraction of porosity,  $\zeta=0, 0.1, 0.2$  and  $0.3$  & gradation index,  $p=0.5, 1$  &  $5$ . It can be observed that the modulus of elasticity of the FG plate without porosity has the highest in magnitude, whereas the FG plate for even-porosity volume fraction  $\zeta = 0.3$  has the lowest in magnitude for all the values of  $p$ . Moreover, at all the porosity volume fractions, the effective modulus of elasticity of perfect FG and FG plate for uneven and logarithmically-uneven distribution matches at the top and bottom of the plate, whereas uneven porosity match with even porosity in the mid surface of the FG plate.

**2.1. Basic assumptions**

The normal and transverse shear deformations contribute significantly in accurately estimating the structural response of FG plates. Hence the present theory considers the influence of normal and transverse shear deformations.

The displacement in the x-direction is  $u$  and y-direction is  $v$  comprises extension, bending and shear components.

$$\bar{u}(x, y) = u(x, y) + u_b(x, y) + u_s(x, y) \quad (2a)$$

$$\bar{v}(x, y) = v(x, y) + v_b(x, y) + v_s(x, y) \quad (2b)$$

Where

$$u_b(x, y) = -zw_{b,x} \quad (2c)$$

$$v_b(x, y) = -zw_{b,y} \quad (2d)$$

$$u_s(x, y) = -\psi(z)w_{s,x} \quad (2e)$$

$$v_s = -\psi(z)w_{s,y} \quad (2f)$$

$$\psi(z) = z - \zeta(z) \quad (2g)$$

$$\zeta(z) = z \text{Cosh}\left(\frac{z}{h}\right) - z \left[ \text{Cosh}\left(\frac{1}{2}\right) + \left(\frac{1}{2}\right) \text{Sinh}\left(\frac{1}{2}\right) \right] \quad (2h)$$

Eq. (2h) represents the novel shear strain function that satisfies the nullity conditions of the transverse shear stress at the upper and lower side of the plate. Thus, this theory doesn't require the shear correction factor. The comma followed by the subscripts represents differentiation with respect to the subscripts throughout the paper.

The transverse displacement  $w$  contains the bending ( $w_b$ ), shear ( $w_s$ ) and through the thickness stretching ( $w_t$ ). The bending and shear components are functions of  $x$  and  $y$  coordinates and the thickness stretching component  $a$  is a function of  $x, y$  and  $z$ .

$$\bar{w} = w_b(x, y) + w_s(x, y) + \zeta(z)_z \xi(x, y, z) \quad (2i)$$

$\xi(x, y, z)$  takes account of influence of normal stress.

The present theory involves only five unknown parameters.

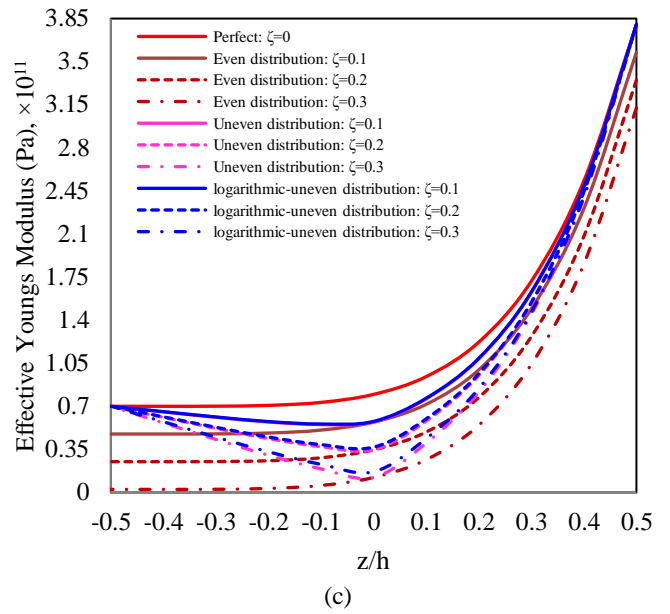
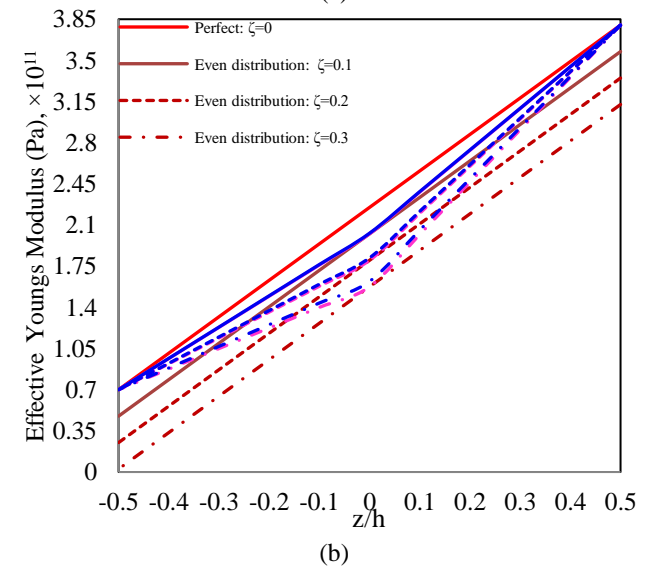
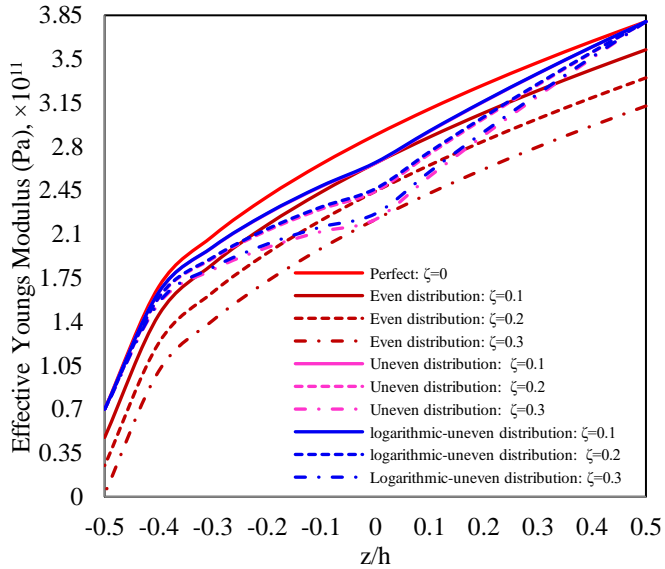


Figure.2. Variation of Modulus of Elasticity of perfect and FG plate with different porosity distributions,  $\zeta=0, 0.1, 0.2$  &  $0.3$ : (a)  $p=0.5$ ; (b)  $p=1$ ; (c)  $p=5$

### 2.2. Strain displacement relations

The necessary equations are derived by assuming the strains are small. The strain displacement relations associated with the displacement model of Eqs. (2a-i), can be applied for thick to thin plates are as follows.

$$\epsilon_{11} = u_{,x} - zw_{b,xx} - \psi(z)w_{s,xx} \quad (3a)$$

$$\epsilon_{22} = v_{,y} - zw_{b,yy} - \psi(z)w_{s,yy} \quad (3b)$$

$$\epsilon_{33} = \zeta(z)_{,zz} \xi \quad (3c)$$

$$\epsilon_{12} = (u_{,y} + v_{,x}) - 2zw_{b,xy} - 2\psi(z)w_{s,xy} \quad (3d)$$

$$\epsilon_{13} = \zeta(z)_{,z}(w_{s,x} + \xi_{,x}) \quad (3e)$$

$$\epsilon_{23} = \zeta(z)_{,z}(w_{s,y} + \xi_{,y}) \quad (3f)$$

### 2.3. Stress-strain relations

The Linear stress-strain relations are given as:

$$s_{11} = Q_{11}\epsilon_{11} + Q_{12}(\epsilon_{22} + \epsilon_{33}) \quad (4a)$$

$$s_{22} = Q_{11}\epsilon_{22} + Q_{12}(\epsilon_{11} + \epsilon_{33}) \quad (4b)$$

$$s_{33} = Q_{11}\epsilon_{33} + Q_{12}(\epsilon_{11} + \epsilon_{22}) \quad (4c)$$

$$(s_{12}, s_{13}, s_{23}) = Q_{66}(\epsilon_{12}, \epsilon_{13}, \epsilon_{23}) \quad (4d)$$

In which,  $s = \{s_{11}, s_{22}, s_{33}, s_{12}, s_{13}, s_{23}\}$  and  $\epsilon = \{\epsilon_{11}, \epsilon_{22}, \epsilon_{33}, \epsilon_{12}, \epsilon_{13}, \epsilon_{23}\}$  are the stresses and strains with regard to the plate coordinating system and

$$Q_{11} = \frac{E(z)(1-\mu)}{(1-2\mu)(1+\mu)} \quad (4e)$$

$$Q_{12} = \frac{\mu E(z)}{(1-2\mu)(1+\mu)} \quad (4f)$$

$$Q_{66} = \frac{E(z)}{2(1+\mu)} \quad (4g)$$

### 2.4. Equilibrium Equations of motion

The static equilibrium equations can be obtained by considering the virtual work and expressed in analytic form as

$$\int_x \int_y \int_z [s_{11}\epsilon_{11} + s_{22}\epsilon_{22} + s_{33}\epsilon_{33} + s_{12}\epsilon_{12} + s_{13}\epsilon_{13} + s_{23}\epsilon_{23}] dx dy dz$$

$$-\int_x \int_y q[\delta w_b + \delta w_s + \zeta(z)_{,z}|^{h/2} \xi] dx dy = 0 \quad (5)$$

or

$$\int_x \int_y [N_1 \delta u_{,x} - M_1 \delta w_{b,xx} - P_1 \delta w_{s,xx} + N_2 \delta v_{,y} - M_2 \delta w_{b,yy} - P_2 \delta w_{s,yy} + S_3 \delta \xi + N_6 (\delta u_{,y} + \delta v_{,x}) - 2M_6 \delta w_{b,xy} - 2P_6 \delta w_{s,xy} + Q_{13} (\delta w_{s,x} + \delta \xi_{,x}) + Q_{23} (\delta w_{s,y} + \delta \xi_{,y}) - q(\delta w_b + \delta w_s + \zeta(z)_{,z}|^{h/2} \xi)] dx dy = 0 \quad (6)$$

In which Ni, Mi, Pi, Si, Qi denotes the forces and moment results which can be defined as follows

$$(N_i, M_i, P_i) = \int_{-h/2}^{h/2} S_{ij}(1, z, \psi(z)) dz, \quad (i, j = 1, 2, 6) \quad (7a)$$

$$S_3 = \int_{-h/2}^{h/2} S_{33} \zeta(z)_{,zz} dz \quad (7b)$$

$$Q_{j3} = \int_{-h/2}^{h/2} S_{j3} \zeta(z)_{,z} dz \quad (7c)$$

The equations of equilibrium are obtained from Eq. (6) by applying the integration by parts to the displacement gradients and putting the coefficients of  $\delta u, \delta v, \delta w_b, \delta w_s$  and  $\delta \xi$  to zero, independently. So, according to this theory, we have

$$\delta u = N_{1,x} + N_{6,y} = 0 \quad (8a)$$

$$\delta v = N_{2,y} + N_{6,x} = 0 \quad (8b)$$

$$\delta w_b = M_{1,xx} + M_{2,yy} + 2M_{6,xy} = -q \quad (8c)$$

$$\delta w_s = P_{1,xx} + P_{2,yy} + 2P_{6,xy} + Q_{13,x} + Q_{23,y} = -q \quad (8d)$$

$$\delta \xi = Q_{13,x} + Q_{23,y} - S_3 = 0 \quad (8e)$$

By putting Eq. (4a-g) into the Eq. (7a-c), and further substitution of the resulting equations into Eq. (8a-e) gives the system of equations in an abbreviated form as:

$$[\Theta]_{5 \times 5} [\Delta]_{5 \times 1} = [F]_{5 \times 1} \quad (9)$$

Where  $[\Theta]$  contains stiffness terms and  $\{\Delta\} = \{u, v, w_b, w_s, \xi\}^t$  denotes the unknown amplitudes and  $\{F\} = \{0, 0, -q, -q, 0\}^t$  is the force matrix.

### 3. Analytical Solutions

In what follows, the solution for the Eq. (9) is obtained by prescribing the simply supported conditions at all the side edges:

$$N_1, M_1, P_1, v, w_b, w_s, w_{b,y}, w_{s,y}, \xi = 0 \text{ at } x = 0, a$$

$$N_2, M_2, P_2, u, w_b, w_s, w_{b,x}, w_{s,x}, \xi = 0 \text{ at } y = 0, b. \quad (10)$$

In accordance with Navier's solution, the external transverse bi-sinusoidal load can be expressed as:

$$q(x, y) = q_{kl} \sin(\varphi x) \sin(\phi y), \quad (k, l = 1, 2, \dots, \infty) \quad (11)$$

Where  $\varphi = \frac{k\pi}{a}, \phi = \frac{l\pi}{b}$ , k and l are the mode numbers. For uniformly distributed, qkl can be defined as:

$$q_{kl} = \begin{cases} \frac{16q}{kl\pi^2}, & \text{for odd k and l} \\ 0, & \text{otherwise} \end{cases} \quad (12)$$

In accordance with Navier's method, the assumed expressions for solutions that satisfy the SS conditions at all the side edges are as follows

$$u(x, y) = u_{kl} \cos(\varphi x) \sin(\phi y) \quad (13a)$$

$$v(x, y) = v_{kl} \sin(\varphi x) \cos(\phi y) \quad (13b)$$

$$[w_b(x, y), w_s(x, y), \xi(x, y)] = [w_{bkl}, w_{skl}, \xi_{kl}] \sin(\varphi x) \sin(\phi y), \quad (k, l = 1, 2, \dots, \infty) \quad (13c)$$

Where  $u_{kl}, v_{kl}, w_{bkl}, w_{skl}, \xi_{kl}$  are the unknowns to be determined.

Substitution of Eqs. (13a-c) into Eqs.(8a-e), the following system of equations in first order are obtained.

$$[\bar{\Theta}]_{5 \times 5} [\bar{\Delta}]_{5 \times 1} = [\bar{F}]_{5 \times 1} \quad (14)$$

The elements of  $[\bar{\Theta}]_{5 \times 5}, [\bar{\Delta}]_{5 \times 1}$  and  $[\bar{F}]_{5 \times 1}$  are given as.

$$\Theta_{11} = -(A_{11} \varphi^2 + A_{66} \phi^2)$$

$$\Theta_{12} = -(A_{12} + A_{66}) \varphi \phi$$

$$\Theta_{13} = B_{11} \varphi^3 + (B_{12} + 2B_{66}) \varphi \phi^2$$

$$\Theta_{14} = B_{11}^S \varphi^3 + (B_{12}^S + 2B_{66}^S) \varphi \phi^2$$

$$\Theta_{14} = E_{11} \varphi$$

$$\Theta_{22} = -(A_{66} \varphi^2 + A_{11} \phi^2)$$

$$\Theta_{23} = B_{11} \phi^3 + (B_{12} + 2B_{66}) \varphi \phi^2$$

$$\Theta_{24} = B_{11}^S \phi^3 + (B_{12}^S + 2B_{66}^S) \varphi \phi^2$$

$$\Theta_{25} = E_{12} \phi$$

$$\Theta_{33} = -D_{11} (\varphi^4 + \phi^4) - (2D_{12} + 4D_{66}) \varphi^2 \phi^2$$

$$\Theta_{34} = -D_{11}^S (\varphi^4 + \phi^4) - (2D_{12}^S + 4D_{66}^S) \varphi^2 \phi^2$$

$$\Theta_{35} = -G_{12} (\varphi^2 + \phi^2)$$

$$\Theta_{44} = -F_{11} (\varphi^4 + \phi^4) - (2F_{12} + 4F_{66}) \varphi^2 \phi^2 - L_{66} (\varphi^2 + \phi^2)$$

$$\Theta_{45} = -J_{12} (\varphi^2 + \phi^2) - L_{66} (\varphi^2 + \phi^2)$$

$$\Theta_{55} = -L_{66} (\varphi^2 + \phi^2) - K_{11}$$

Where  $(A_{ij}|B_{ij}|D_{ij}|B_{ij}^S|D_{ij}^S|F_{ij}|E_{ij}|G_{ij}|J_{ij}|K_{ij}|L_{ij}) = \int_{-h/2}^{h/2} Q_{ij}(1|z|z^2|\psi(z)|z\psi(z)|\psi(z)^2|\zeta(z)_{,zz}|z\zeta(z)_{,zz}|\psi(z)\zeta(z)_{,zz}|\zeta(z)_{,zz}^2|\zeta(z)_{,z}^2) dz$   $(i, j = 1, 2, 6)$

$$\{\bar{\Delta}\} = \{u_{kl}, v_{kl}, w_{bkl}, w_{skl}, \xi_{kl}\}^t$$

$$\{\bar{F}\} = \{0, 0, -q_{kl}, -q_{kl}, 0\}^t$$

### 4. Results and Discussion

The flexural response of simply supported perfect and porous FG rectangular plates subjected to transverse bi-sinusoidal load is investigated. In the present paper, ceramic-metal FG plates are considered, and their material properties are:

Metal (Aluminium, Al): Modulus of Elasticity (Em)= 70 GPa, Ceramic (Alumina, Al<sub>2</sub>O<sub>3</sub>): Modulus of Elasticity (Ec)= 380 GPa and Poisson's ratio ( $\mu$ ) is assumed as 0.3.

The displacements and stresses assessed here are reported using the following dimensionless forms:

$$W = w \left( \frac{a}{2}, \frac{b}{2}, z \right) \frac{10E_c h^3}{q_{kl} a^4} \quad (15a)$$

$$S_{11} = s_{11} \left( \frac{a}{2}, \frac{b}{2}, z \right) \frac{h^2}{q_{kl} a^2} \quad (15b)$$

$$S_{22} = s_{22} \left( \frac{a}{2}, \frac{b}{2}, z \right) \frac{h^2}{q_{kl} a^2} \quad (15c)$$

$$S_{33} = s_{33} \left( \frac{a}{2}, \frac{b}{2}, z \right) \frac{h^2}{q_{kl} a^2} \quad (15d)$$

$$S_{13} = s_{13} \left( 0, \frac{b}{2}, z \right) \frac{h}{q_{kl} a} \quad (15e)$$

To validate the present theory, dimensionless center deflections and stresses of exponentially graded plates are compared with: (i) 3-D exact solutions of the perfect plate [20]; (ii) Novel higher order theory, which includes new trigonometric shear strain shape function developed by Mantari et al. [21] and (iii) A Quasi-3D refined theory developed by Zenkour [8] for single layer and sandwich plates with porosities.

It should be noted that 3-D elasticity solutions [20] and solutions of the higher order theory [21] were obtained on the basis of trigonometric variation of both in-plane and transverse displacements along the thickness, whereas solutions of a Quasi-3D higher order theory [8] were obtained on the basis of polynomial type shear strain shape function with six unknowns.

Table 1 consists results of dimensionless transverse center deflection  $W$  with and without inclusion of the porosity volume fraction; normal stress  $S_{22}$  and transverse shear stress  $S_{13}$  (without inclusion of porosity volume fraction) of exponentially graded plates for different thickness ratios ( $a/h$ ) and exponents  $p$ .

From the Table 1; it is observed that the present results without considering the porosity are agreeing well with the 3-D elasticity solutions and the results provided by Mantari et al. [21] and

Zenkour [8]. This point to the use of new shear strain shape function given in Eq. (2h) has an utmost effect on the accuracy of the results.

The additional results of dimensionless transverse center deflections, and stresses in FG square plates with even, uneven and Logarithmically-uneven porosity models are reported in Tables 2-6 for perfect and porous FG plates.

From Tables 2-6, it should be noted that, the increase of volume fraction of porosity increases the dimensionless transverse deflection and axial stress & decreases the transverse shear stresses. The reason for this is an increase in the volume fraction of porosity ( $\zeta$ ) results in a decrease in the Young's modulus of the plate. The dimensionless deflections decrease with the increase of

$a/h$ , and increases with increase of  $p$ . The stresses increase as  $b/a$  ratio increase. We can say that the thickness ratio  $a/h$ , aspect ratio  $b/a$ , gradation index and porosity volume fraction have a considerable influence on the deflections and stresses for three types of distributions.

It is also noticed from Table 6 that no variation of transverse shear stresses for a completely ceramic and metallic plate for all kinds of porosity models. The reason is that the plate is completely homogeneous in all the cases. The effect of shear component is to decrease the deflections with increase of side-to-thickness ratios. It is because; the shear deformation is more noticeable in thick plates.

Table 1: Comparison study of dimensionless center deflections, axial and transverse shear stress of perfect and porous FG plate subjected to sinusoidal load for various exponents and aspect ratios.

a/h			p=0.1	p=0.3	p=0.5	p=0.7	p=1.0	p=1.5		
W	2	3-D [15]	0.57693	0.52473	0.47664	0.4324	0.37269	0.28904		
		Mantari et al[16]	0.57789	0.5224	0.47179	0.42567	0.36485	0.27939		
		Zenkour( $\xi=0$ )[3]	0.5751	0.5199	0.4695	0.4236	0.3624	0.2781		
		Present	0.5782	0.5227	0.4721	0.4259	0.3644	0.2795		
		Zenkour ( $\xi=0.1$ ) [3]	0.7182	0.6493	0.5864	0.5291	0.4526	0.3473		
		Present ( $\xi=0.1$ )	0.7221	0.6528	0.5895	0.5319	0.455	0.3491		
	4	3-D [15]	0.349	0.31677	0.28747	0.26083	0.22534	0.18054		
		Mantari et al[16]	0.3486	0.31519	0.28477	0.2571	0.22028	0.1697		
		Zenkour( $\xi=0$ ) [3]	0.3481	0.3148	0.2844	0.2568	0.22	0.1695		
		Present	0.3486	0.3152	0.2848	0.2571	0.2203	0.16972		
		S <sub>22</sub>	2	3-D [15]	0.31032	0.32923	0.34953	0.37127	0.40675	0.47405
		Mantari et al[16]		0.29244	0.31468	0.33826	0.36325	0.40405	0.47848	
Present	0.292164	0.314372		0.337924	0.362878	0.403065	0.477919			
4	3-D [15]	0.22472		0.23995	0.25621	0.27356	0.30177	0.35885		
	Mantari et al[16]	0.22372		0.23907	0.25544	0.27291	0.30137	0.35555		
	Present	0.222852		0.238118	0.254404	0.271791	0.300126	0.354105		
S <sub>13</sub>	10	Mantari et al[16]	0.238	0.2376	0.2368	0.2356	0.233	0.2268		
		Present	0.237453	0.237042	0.236223	0.234999	0.232423	0.226237		

Table 2: Effect of volume fraction exponent, porosity distribution, porosity volume fraction and side to thickness ratio on Dimensionless center deflection in FG plate

p	$\zeta$	a/h=2			a/h=4			a/h=10		
		Even	Uneven	Logarithmically Uneven	Even	Uneven	Logarithmically Uneven	Even	Uneven	Logarithmically Uneven
0	0	0.6079	0.6079	0.6079	0.3665	0.3665	0.3665	0.2942	0.2942	0.2942
	0.1	0.6462	0.6266	0.6262	0.3896	0.3745	0.3743	0.3128	0.2991	0.2989
	0.2	0.6896	0.6467	0.6448	0.4157	0.3829	0.3821	0.3338	0.3041	0.3036
	0.3	0.7393	0.6684	0.6638	0.4457	0.3918	0.39	0.3578	0.3092	0.3082
1	0	1.0994	1.0994	1.0994	0.6916	0.6916	0.6916	0.5695	0.5695	0.5695
	0.1	1.245	1.1625	1.1608	0.792	0.7237	0.7228	0.6563	0.5925	0.5919
	0.2	1.442	1.2344	1.2273	0.9323	0.7598	0.7562	0.7797	0.618	0.6155
	0.3	1.73	1.3174	1.2994	1.1474	0.8008	0.792	0.9731	0.6467	0.6406
2	0	1.4725	1.4725	1.4725	0.8947	0.8947	0.8947	0.7225	0.7225	0.7225
	0.1	1.7575	1.5972	1.5939	1.087	0.957	0.9554	0.8871	0.7664	0.7653
	0.2	2.2142	1.7489	1.7333	1.4186	1.0321	1.0244	1.1815	0.819	0.8136
	0.3	3.1694	1.9381	1.8956	2.2084	1.1249	1.1042	1.9217	0.8834	0.869

5	0	2.1224	2.1224	2.1224	1.1597	1.1597	1.1597	0.8741	0.8741	0.8741
	0.1	2.7553	2.4299	2.4212	1.5032	1.2833	1.2799	1.1319	0.9434	0.9415
	0.2	4.0171	2.866	2.8174	2.2426	1.4521	1.4336	1.7166	1.0331	1.0235
	0.3	9.3463	3.5402	3.3734	6.7116	1.7023	1.6414	5.931	1.1567	1.1276
10	0	2.5286	2.5286	2.5286	1.3355	1.3355	1.3355	0.9815	0.9815	0.9815
	0.1	3.4679	3.0000	2.9861	1.7831	1.5047	1.4998	1.2838	1.0616	1.0594
	0.2	5.6813	3.7539	3.6641	2.8284	1.7597	1.7301	1.9836	1.1686	1.1569
	0.3	20.9018	5.1882	4.796	12.6446	2.2146	2.0929	10.1713	1.3292	1.2893
$\infty$	0	3.3003	3.3003	3.3003	1.9896	1.9896	1.9896	1.5973	1.5973	1.5973
	0.1	4.8636	3.9581	3.9384	2.9321	2.2587	2.251	2.3539	1.7522	1.748
	0.2	9.2408	5.0546	4.9204	5.571	2.6606	2.6138	4.4724	1.95	1.9289
	0.3	92.4079	7.3876	6.7098	55.7098	3.4109	3.2022	44.7236	2.2323	2.1628

Table 3: Effect of volume fraction exponent, porosity distribution and porosity volume fraction on dimensionless axial stress in FG plate,  $a/h=2$

$p$	$\zeta$	Even				Uneven				Logarithmically-Uneven			
		$b/a=1$	$b/a=2$	$b/a=3$	$b/a=4$	$b/a=1$	$b/a=2$	$b/a=3$	$b/a=4$	$b/a=1$	$b/a=2$	$b/a=3$	$b/a=4$
0	0	0.2815	0.4987	0.5884	0.6278	0.2815	0.4987	0.5884	0.6278	0.2815	0.4987	0.5884	0.6278
	0.1	0.2815	0.4987	0.5884	0.6278	0.2868	0.5076	0.5987	0.6387	0.2867	0.5074	0.5984	0.6385
	0.2	0.2815	0.4987	0.5884	0.6278	0.2923	0.5168	0.6094	0.6501	0.2917	0.516	0.6084	0.6491
	0.3	0.2815	0.4987	0.5884	0.6278	0.298	0.5265	0.6207	0.6621	0.2968	0.5245	0.6183	0.6596
1	0	0.4444	0.7806	0.9198	0.981	0.4444	0.7806	0.9198	0.981	0.4444	0.7806	0.9198	0.981
	0.1	0.4685	0.8239	0.971	1.0357	0.4586	0.8042	0.9472	1.0101	0.4582	0.8036	0.9465	1.0093
	0.2	0.5026	0.8857	1.0442	1.1139	0.474	0.8298	0.9769	1.0416	0.4725	0.8273	0.974	1.0385
	0.3	0.5553	0.983	1.1595	1.2371	0.4911	0.8579	1.0094	1.076	0.4875	0.8519	1.0025	1.0687
2	0	0.5314	0.9292	1.0933	1.1654	0.5314	0.9292	1.0933	1.1654	0.5314	0.9292	1.0933	1.1654
	0.1	0.5812	1.0191	1.1995	1.2787	0.5548	0.9676	1.1377	1.2125	0.5542	0.9666	1.1366	1.2113
	0.2	0.6652	1.1748	1.3842	1.4761	0.5819	1.0116	1.1884	1.2661	0.5792	1.0072	1.1834	1.2607
	0.3	0.8594	1.55	1.8321	1.9557	0.6137	1.063	1.2474	1.3284	0.6067	1.0517	1.2346	1.3148
5	0	0.6592	1.137	1.3333	1.4196	0.6592	1.137	1.3333	1.4196	0.6592	1.137	1.3333	1.4196
	0.1	0.7483	1.2866	1.5073	1.6042	0.7019	1.2008	1.4054	1.4952	0.7008	1.1991	1.4035	1.4932
	0.2	0.9198	1.5827	1.853	1.9715	0.7579	1.2821	1.4962	1.5901	0.7519	1.2735	1.4866	1.5801
	0.3	1.7245	3.1501	3.7245	3.9755	0.8385	1.3953	1.6213	1.7202	0.819	1.3682	1.5915	1.6893
10	0	0.7763	1.3467	1.5815	1.6846	0.7763	1.3467	1.5815	1.6846	0.7763	1.3467	1.5815	1.6846
	0.1	0.8989	1.5486	1.8153	1.9324	0.8338	1.4313	1.6765	1.7841	0.8322	1.429	1.6739	1.7814
	0.2	1.1426	1.9432	2.2697	2.4129	0.916	1.5468	1.8042	1.917	0.9067	1.5339	1.79	1.9023
	0.3	2.5893	4.4839	5.2393	5.5684	1.0586	1.7378	2.0122	2.1322	1.0205	1.6875	1.9577	2.0759

Table 4: Effect of volume fraction exponent, porosity distribution and porosity volume fraction on dimensionless axial stress in FG plate,  $a/h=4$

$p$	$\zeta$	Even				Uneven				Logarithmically-Uneven			
		$b/a=1$	$b/a=2$	$b/a=3$	$b/a=4$	$b/a=1$	$b/a=2$	$b/a=3$	$b/a=4$	$b/a=1$	$b/a=2$	$b/a=3$	$b/a=4$
0	0	0.2156	0.4348	0.5249	0.5645	0.2156	0.4348	0.5249	0.5645	0.2156	0.4348	0.5249	0.5645
	0.1	0.2156	0.4348	0.5249	0.5645	0.2191	0.4417	0.5332	0.5734	0.219	0.4416	0.533	0.5732
	0.2	0.2156	0.4348	0.5249	0.5645	0.2228	0.4489	0.5418	0.5826	0.2224	0.4482	0.541	0.5818
	0.3	0.2156	0.4348	0.5249	0.5645	0.2266	0.4563	0.5507	0.5922	0.2258	0.4548	0.5489	0.5902
1	0	0.333	0.6726	0.8126	0.8742	0.333	0.6726	0.8126	0.8742	0.333	0.6726	0.8126	0.8742
	0.1	0.3521	0.7111	0.859	0.924	0.3421	0.6905	0.8341	0.8972	0.3419	0.6901	0.8335	0.8966
	0.2	0.3798	0.7668	0.9261	0.9961	0.352	0.7096	0.857	0.9218	0.351	0.7078	0.8548	0.9194

	0.3	0.4244	0.8562	1.0337	1.1116	0.3626	0.7302	0.8816	0.9482	0.3603	0.7258	0.8764	0.9426
2	0	0.3928	0.7906	0.9545	1.0265	0.3928	0.7906	0.9545	1.0265	0.3928	0.7906	0.9545	1.0265
	0.1	0.4325	0.8699	1.0498	1.1288	0.4073	0.8185	0.9877	1.0621	0.4069	0.8178	0.9869	1.0612
	0.2	0.5039	1.0123	1.2209	1.3125	0.4237	0.8496	1.0249	1.1019	0.422	0.8465	1.0212	1.098
	0.3	0.685	1.3736	1.6546	1.7778	0.4424	0.8851	1.0671	1.1471	0.4384	0.8774	1.058	1.1373
5	0	0.4695	0.9396	1.1332	1.2183	0.4695	0.9396	1.1332	1.2183	0.4695	0.9396	1.1332	1.2183
	0.1	0.5287	1.0547	1.2711	1.3662	0.4896	0.9756	1.1756	1.2636	0.4891	0.9746	1.1746	1.2624
	0.2	0.6511	1.2925	1.5555	1.671	0.5135	1.0167	1.2238	1.3147	0.511	1.0126	1.2189	1.3096
	0.3	1.4132	2.8063	3.3701	3.6167	0.5439	1.0664	1.2811	1.3754	0.5369	1.0552	1.2683	1.3619
10	0	0.5595	1.1227	1.3549	1.4569	0.5595	1.1227	1.3549	1.4569	0.5595	1.1227	1.3549	1.4569
	0.1	0.6359	1.2715	1.5334	1.6485	0.5848	1.1676	1.4077	1.5132	0.5841	1.1664	1.4063	1.5118
	0.2	0.7818	1.5493	1.865	2.0037	0.6156	1.2184	1.4666	1.5757	0.6124	1.2133	1.4607	1.5695
	0.3	1.8652	3.6278	4.3407	4.6525	0.66	1.2839	1.5403	1.6529	0.6489	1.2682	1.5229	1.6348

Table 5: Effect of volume fraction exponent, porosity distribution and porosity volume fraction on dimensionless axial stress in FG plate,  $a/h=10$

p	$\zeta$	Even				Uneven				Logarithmically-Uneven			
		$b/a=1$	$b/a=2$	$b/a=3$	$b/a=4$	$b/a=1$	$b/a=2$	$b/a=3$	$b/a=4$	$b/a=1$	$b/a=2$	$b/a=3$	$b/a=4$
0	0	0.1988	0.4183	0.5085	0.5481	0.1988	0.4183	0.5085	0.5481	0.1988	0.4183	0.5085	0.5481
	0.1	0.1988	0.4183	0.5085	0.5481	0.2019	0.4247	0.5163	0.5565	0.2018	0.4245	0.5161	0.5563
	0.2	0.1988	0.4183	0.5085	0.5481	0.205	0.4313	0.5242	0.5651	0.2047	0.4306	0.5235	0.5642
	0.3	0.1988	0.4183	0.5085	0.5481	0.2083	0.438	0.5325	0.5739	0.2076	0.4366	0.5308	0.5721
1	0	0.3047	0.6448	0.7849	0.8465	0.3047	0.6448	0.7849	0.8465	0.3047	0.6448	0.7849	0.8465
	0.1	0.3225	0.682	0.83	0.8951	0.3124	0.6611	0.8047	0.8678	0.3122	0.6606	0.8042	0.8673
	0.2	0.3486	0.7361	0.8956	0.9657	0.3206	0.6783	0.8257	0.8905	0.3198	0.6767	0.8237	0.8883
	0.3	0.3912	0.8235	1.0011	1.0792	0.3294	0.6968	0.8481	0.9146	0.3276	0.6929	0.8434	0.9095
2	0	0.3568	0.7542	0.9179	0.9898	0.3568	0.7542	0.9179	0.9898	0.3568	0.7542	0.9179	0.9898
	0.1	0.3938	0.8306	1.0103	1.0892	0.3687	0.779	0.948	1.0222	0.3684	0.7784	0.9472	1.0214
	0.2	0.4618	0.9693	1.1776	1.2691	0.382	0.8065	0.9813	1.0581	0.3807	0.8038	0.978	1.0545
	0.3	0.6392	1.3267	1.6074	1.7304	0.397	0.8374	1.0187	1.0983	0.3937	0.8307	1.0106	1.0897
5	0	0.4188	0.8865	1.0792	1.164	0.4188	0.8865	1.0792	1.164	0.4188	0.8865	1.0792	1.164
	0.1	0.4695	0.9918	1.207	1.3016	0.4323	0.9144	1.1132	1.2006	0.4319	0.9137	1.1123	1.1997
	0.2	0.5777	1.2129	1.474	1.5886	0.4466	0.9439	1.149	1.2391	0.4452	0.9411	1.1455	1.2354
	0.3	1.3267	2.711	3.2718	3.5172	0.462	0.9751	1.1867	1.2797	0.4588	0.9686	1.1788	1.2712
10	0	0.5014	1.0623	1.2937	1.3954	0.5014	1.0623	1.2937	1.3954	0.5014	1.0623	1.2937	1.3954
	0.1	0.5646	1.1961	1.4566	1.5711	0.5172	1.0956	1.3343	1.4392	0.5168	1.0948	1.3333	1.4382
	0.2	0.6819	1.4404	1.753	1.8904	0.5326	1.1277	1.3734	1.4814	0.5312	1.1248	1.3698	1.4776
	0.3	1.6548	3.3827	4.0841	4.3912	0.5471	1.1562	1.4077	1.5184	0.5442	1.1508	1.4013	1.5114

Table 6: Effect of volume fraction exponent, porosity distribution and volume fraction of porosity on Dimensionless transverse shear stress in FG plate,  $a/h=10$

p	$\zeta$	Even				Uneven				Logarithmically-Uneven			
		$b/a=1$	$b/a=2$	$b/a=3$	$b/a=4$	$b/a=1$	$b/a=2$	$b/a=3$	$b/a=4$	$b/a=1$	$b/a=2$	$b/a=3$	$b/a=4$
0	0	0.2375	0.3801	0.4276	0.4472	0.2375	0.3801	0.4276	0.4472	0.2375	0.3801	0.4276	0.4472
	0.1	0.2375	0.3801	0.4276	0.4472	0.2326	0.3723	0.4188	0.4380	0.2327	0.3725	0.4190	0.4382
	0.2	0.2375	0.3801	0.4276	0.4472	0.2273	0.3638	0.4093	0.4280	0.2278	0.3646	0.4102	0.4290
	0.3	0.2375	0.3801	0.4276	0.4472	0.2215	0.3545	0.3989	0.4171	0.2227	0.3565	0.4011	0.4194
2	0	0.2174	0.3480	0.3915	0.4095	0.2174	0.3480	0.3915	0.4095	0.2174	0.3480	0.3915	0.4095
	0.1	0.2139	0.3424	0.3852	0.4028	0.2032	0.3252	0.3659	0.3827	0.2036	0.3258	0.3666	0.3834

	0.2	0.2087	0.3340	0.3757	0.3929	0.1858	0.2973	0.3345	0.3498	0.1876	0.3002	0.3378	0.3532
	0.3	0.1993	0.3190	0.3589	0.3754	0.1639	0.2623	0.2951	0.3086	0.1688	0.2702	0.3040	0.3179
5	0	0.1917	0.3069	0.3452	0.3610	0.1917	0.3069	0.3452	0.3610	0.1917	0.3069	0.3452	0.3610
	0.1	0.1785	0.2857	0.3214	0.3362	0.1630	0.2609	0.2935	0.3069	0.1638	0.2622	0.2950	0.3085
	0.2	0.1538	0.2462	0.2770	0.2897	0.1214	0.1944	0.2187	0.2287	0.1261	0.2018	0.2271	0.2375
	0.3	0.0872	0.1395	0.1570	0.1642	0.0554	0.0887	0.0998	0.1044	0.0719	0.1152	0.1296	0.1355
10	0	0.2101	0.3363	0.3784	0.3957	0.2101	0.3363	0.3784	0.3957	0.2101	0.3363	0.3784	0.3957
	0.1	0.2006	0.3211	0.3613	0.3778	0.1777	0.2844	0.3200	0.3346	0.1786	0.2859	0.3217	0.3364
	0.2	0.1789	0.2864	0.3222	0.3370	0.1247	0.1996	0.2246	0.2348	0.1310	0.2098	0.2360	0.2468
	0.3	0.0616	0.0987	0.1110	0.1161	0.0206	0.0330	0.0371	0.0388	0.0494	0.0791	0.0890	0.0931
$\infty$	0	0.2375	0.3801	0.4276	0.4472	0.2375	0.3801	0.4276	0.4472	0.2375	0.3801	0.4276	0.4472
	0.1	0.2375	0.3801	0.4276	0.4472	0.2052	0.3284	0.3695	0.3864	0.2062	0.3300	0.3712	0.3882
	0.2	0.2375	0.3801	0.4276	0.4472	0.1492	0.2388	0.2686	0.2809	0.1562	0.2499	0.2812	0.2941
	0.3	0.2375	0.3801	0.4276	0.4472	0.0243	0.0390	0.0438	0.0458	0.0612	0.0980	0.1102	0.1153

Figure 3 shows the through-the-thickness distribution of dimensionless deflections of square FG plate in the thickness direction for  $a/h=10$  with several values of  $p$  and  $\zeta$ .

From Figure 3a it is seen that the deflection increases as  $p$  increases for  $\zeta = 0$ . The influence of porosity distribution and the volume fraction of porosity are illustrated in Figures 3b-d. The increase of  $\zeta$  value increases the deflection. The maximum center deflection occurs at the plate center for all types of porosity distributions and porosity volume fractions and varies symmetrically about the mid plane through-the-thickness of the plate for fixed  $p=0.5$  (see Figures 3b-d). However the maximum center deflection hasn't occurred at the plate center for perfect FG plates. This is because of the inhomogeneity of the plate material. Also seen that, the even porosity distribution shows larger deflection compared to uneven and logarithmically-uneven distribution values in the thickness direction of all porosity volume fractions.

The distribution of dimensionless axial stress  $S_{11}$  of very thick ( $a/h=4$ ) rectangular ( $b/a=3$ ) FG plate in the thickness direction is portrayed in Figure 4 for several values of  $p$  and  $\zeta$ . The axial stresses are tensile and compressive at the upper and lower surface of the plate respectively, for three types of distributions and porosity volume fraction values. The increase of the porosity volume fraction results in increase of axial stress. This can be defended by the fact that the porosity lessens the rigidity of the plate. From Figure 4a, it is noteworthy to see that the stress increases with increase of exponent  $p$ . The difference in axial stress is more in even distribution compared to other two distributions. The volume fraction of porosity  $\zeta$  of even porosity distribution (see Figure 4b) has no influence on axial stress in two positions,  $S_{11}=-0.26$  at  $z/h=-0.23$  and  $S_{11}=0.31$  at  $z/h=0.325$ . Whereas the porosity volume fraction  $\zeta$  of uneven (see Figure 4c) and logarithmic-uneven (see Figure 4d) porosity distribution has

no influence on axial stress in three positions,  $S_{11}=-0.37$  at  $z/h=-0.2711$ ,  $S_{11}=0.05$  at  $z/h=-0.1211$  and  $S_{11}=0.5$  at  $z/h=0.39$ . &  $S_{11}=0.27$  at  $z/h=-0.365$ ,  $S_{11}=-0.1291$  at  $z/h=0.045$  and  $S_{11}=0.52$  at  $z/h=0.39$  respectively.

The distribution of normal stress  $S_{33}$  in the thickness direction of very thick ( $a/h=4$ ) rectangular ( $b/a=3$ ) FG plate is shown in Fig. 5 for several values of  $p$  and  $\zeta$ . The volume fraction of porosity has no influence on normal stress  $S_{33}$  in three positions for uneven and Logarithmically-uneven distribution (see Figures. 5c-5d) respectively, are  $S_{33}=-0.0677$  at  $z/h=-0.3$ ,  $S_{33}=-0.0697$  at  $z/h=0.06$ ,  $S_{33}=0.016$  at  $z/h=0.45$  &  $S_{33}=-0.0677$  at  $z/h=-0.29$ ,  $S_{33}=-0.066$  at  $z/h=0.07$ ,  $S_{33}=0.016$ , at  $z/h=0.45$ .

Lastly, Figure 6 illustrates the distribution of dimensionless transverse shear stress  $S_{13}$  of FG rectangular ( $b/a=3$ ) in the thickness direction for  $a/h=4$  with different values of  $p$  and  $\zeta$ . The transverse shear stress  $S_{13}$  increases as  $p=0, 1$  and  $2$  while it decreases as  $p=5$  and  $10$  (see Figure. 6a). The maximum values of transverse shear stress for perfect, even, uneven and logarithmic-uneven distributions at  $p=2$  respectively, are  $S_{13}=0.4962$  at  $z/h=0.2$ ,  $S_{13}=0.5835$  at  $z/h=0.2$  and  $\zeta = 0.2$ ,  $S_{13} =0.5752$  at  $z/h=0.2$  and  $\zeta = 0.3$  &  $S_{13} =0.5645$  at  $z/h=0.3$  and  $\zeta = 0.3$  (see Figures. 5a-d). From Figures 6b-d, it is observed that the transverse shear stress increases as  $\zeta$  increases. The porosity volume fraction  $\zeta$  of even porosity distribution (see Figure. 6b) has no influence on transverse shear stress in one position,  $S_{13}=0.4325$  at  $z/h=0.05$ . Whereas the porosity volume fraction  $\zeta$  of uneven (see Figure. 6c) and logarithmic-uneven (see Figure. 6d) porosity distribution has no influence on transverse shear stress in two positions respectively, are  $S_{13}=0.114$  at  $z/h=-0.3375$ ,  $S_{13}=0.468$  at  $z/h=0.11$  &  $S_{13}=0.115$  at  $z/h=-0.34$   $S_{13}=0.47$  at  $z/h=0.115$ .

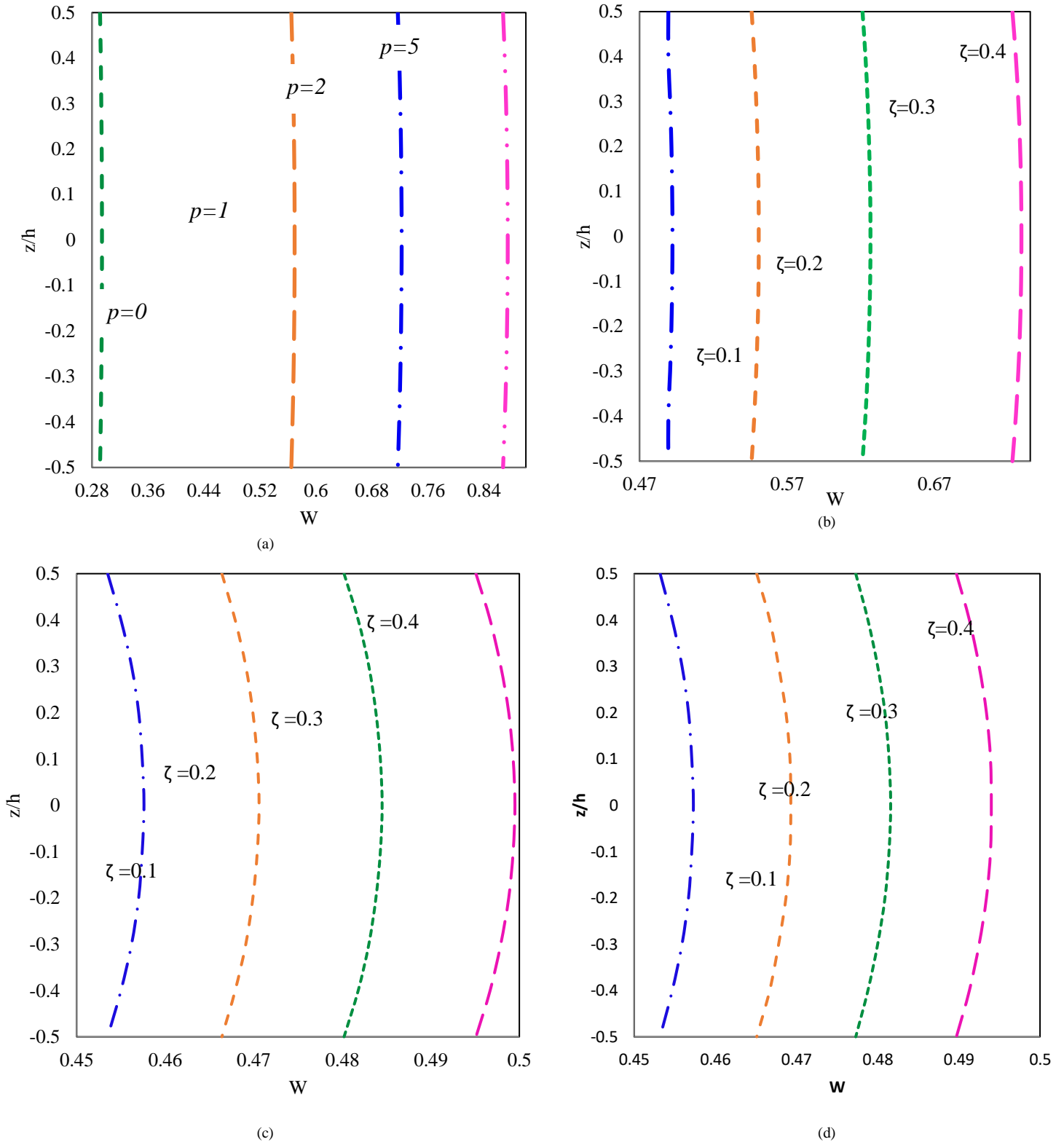
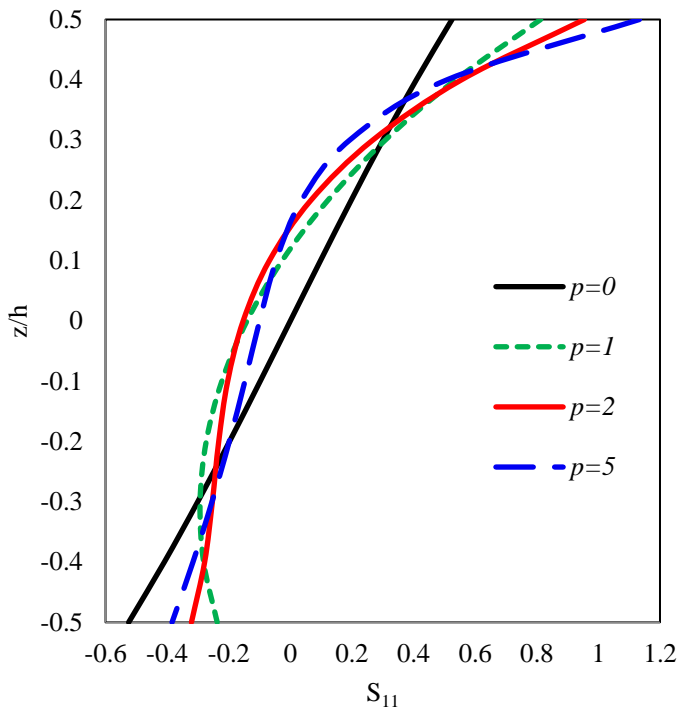
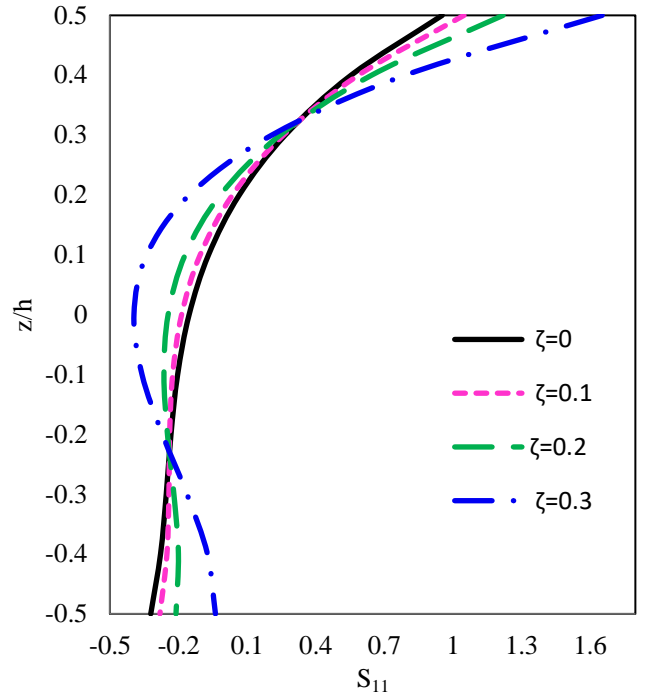


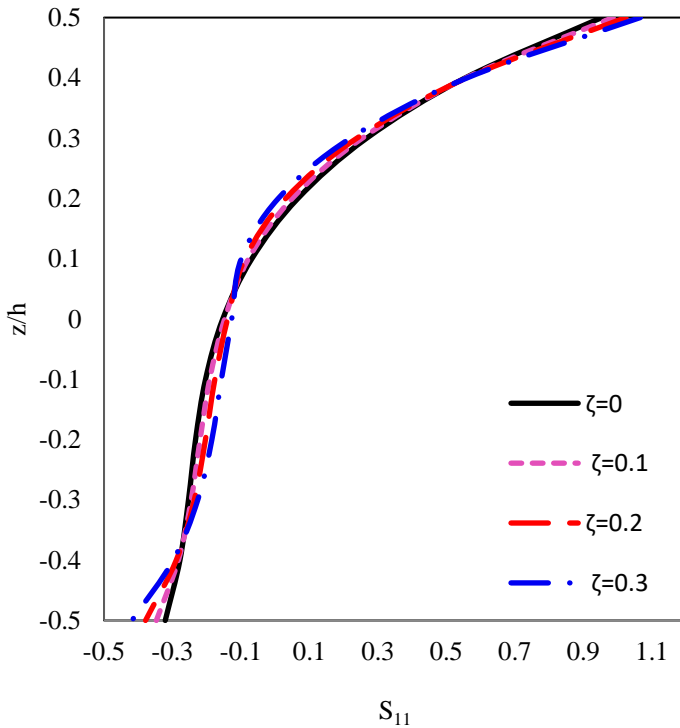
Figure 3. Distributions of dimensionless deflection through the thickness of square (a) perfect FG plate; (b) FG Plate with Even porosity distribution; (c) FG Plate with the uneven porosity distribution; (d) FG Plate with Logarithmic-uneven porosity distribution for  $p=0.5$  ( $a/h=10$ )



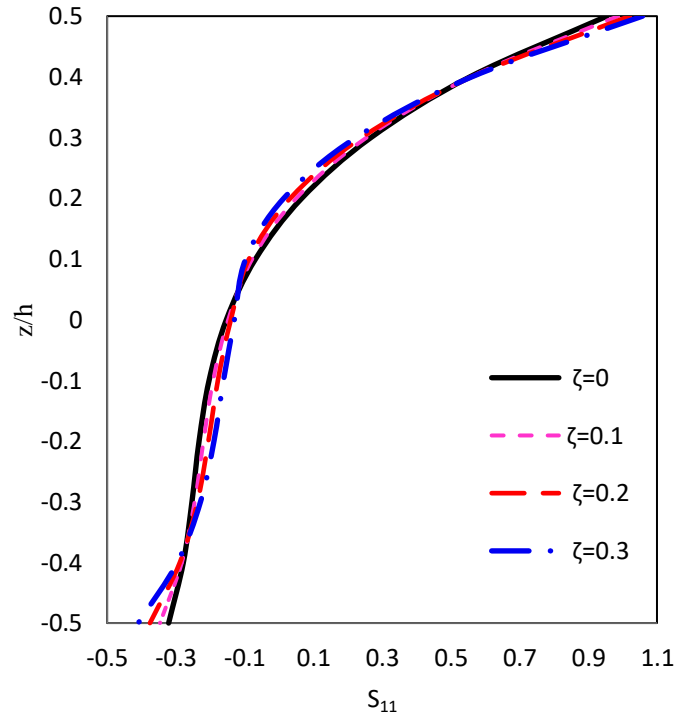
(a)



(b)

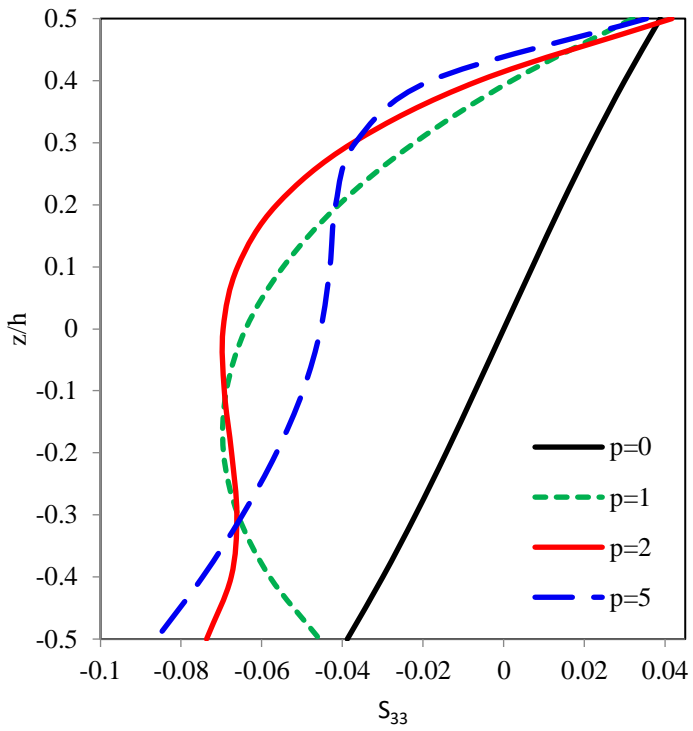


(c)

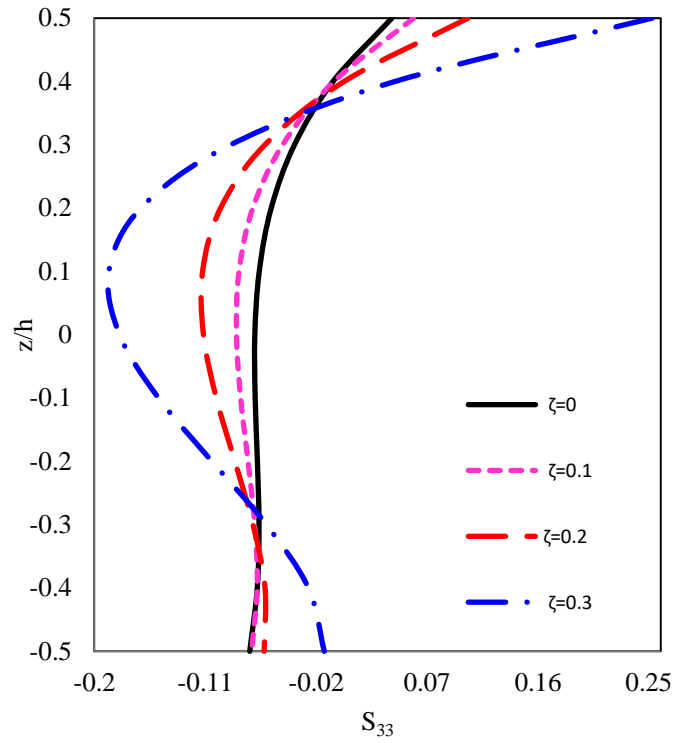


(d)

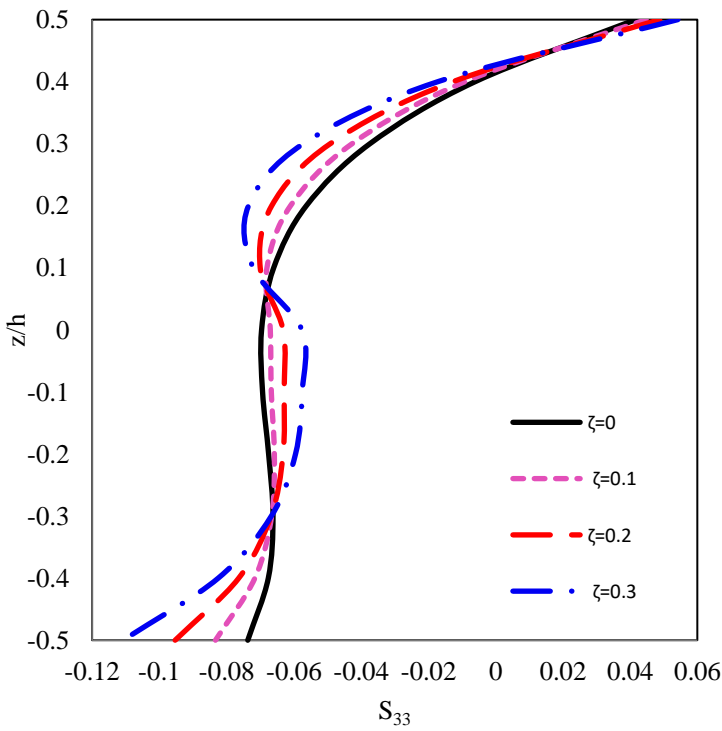
Figure.4. Distributions of dimensionless axial stress through the thickness of Rectangular ( $b/a=3$ ) (a) perfect FG plate; and (b) FG plate with the Even porosity distribution; (c) FG plate with the uneven porosity distribution; (d) FG plate with Logarithmic-uneven porosity distribution for  $p=2$  ( $a/h=4$ )



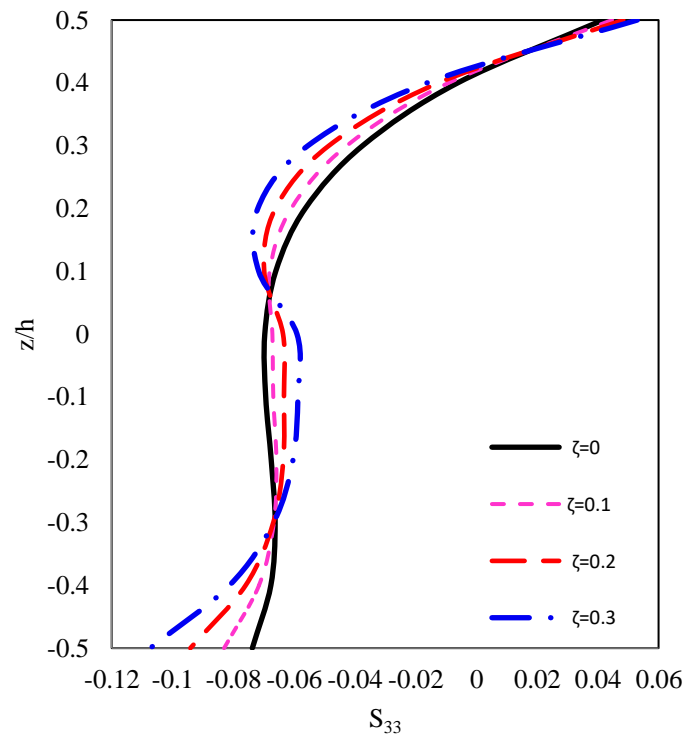
(a)



(b)



(c)



(d)

Fig.5. Distributions of dimensionless normal stress  $S_{33}$  through the thickness of Rectangular ( $b/a=3$ ) (a) perfect FG plate; and (b) FG plate with the Even porosity distribution; (c) FG plate with the uneven porosity distribution; (d) FG plate with Logarithmic-uneven porosity distribution for  $p=2$  ( $a/h=4$ )

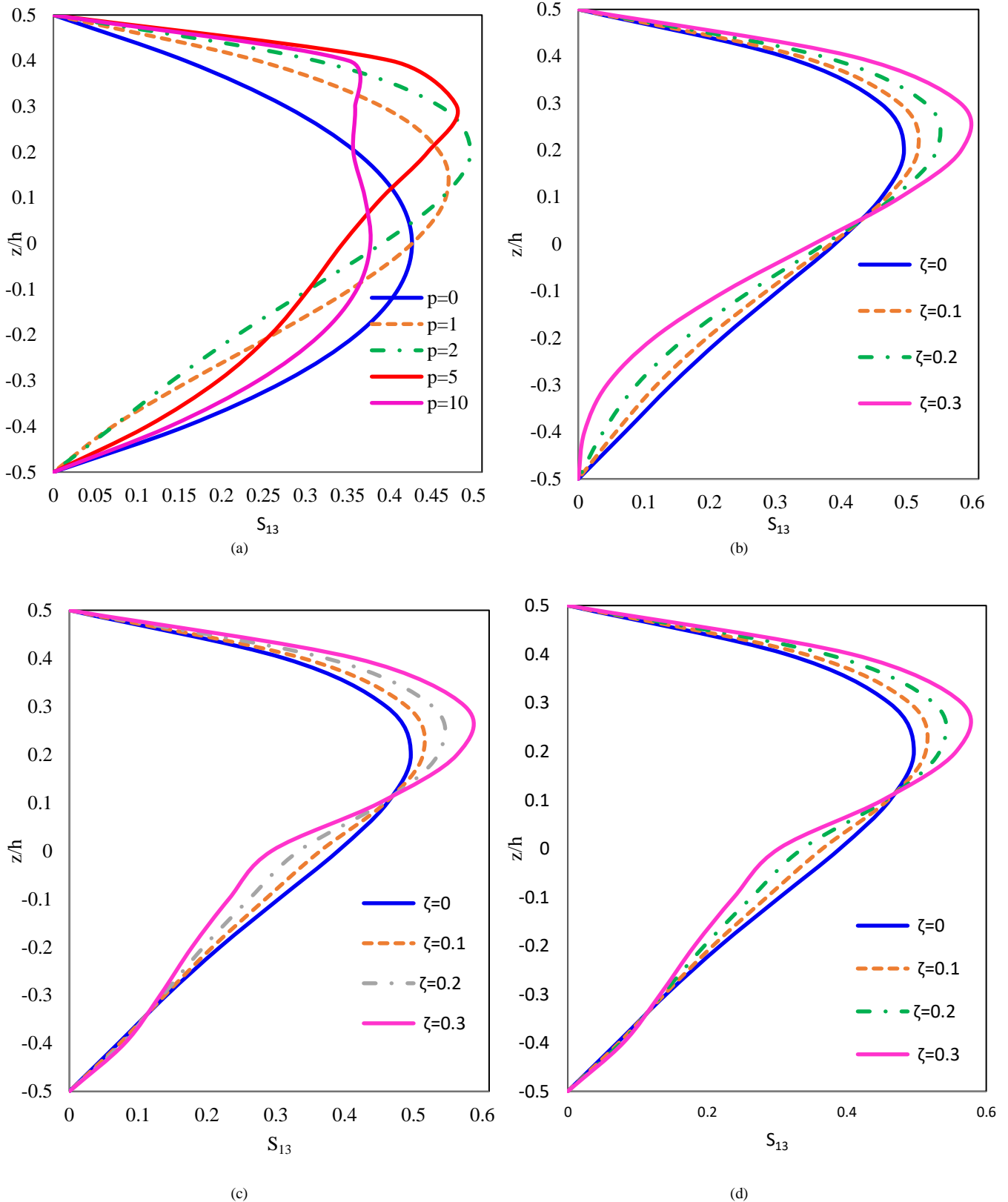


**Figure 6.** Distributions of dimensionless Transverse shear stress through the thickness of Rectangular ( $b/a=3$ ) (a) perfect FG plate; and (b) FG plate with the Even porosity distribution; (c) FG plate with the uneven porosity distribution; (d) FG plate with Logarithmic-uneven porosity distribution for  $p=2$  ( $a/h=4$ )

### 5. Conclusions

A novel higher order theory is developed by considering the thickness stretching of ceramic/metal single-layered FG plates. This theory fulfills the nullity conditions at the top and bottom surfaces of the FG plate for the transverse shear stresses and thus

eliminates the use of a shear correction factor. The equilibrium equations are derived by employing the principle of virtual displacements. Then, the analytical solutions are presented for porous FG plates under all sides are simply supported conditions. The even, uneven and logarithmically-uneven porosity distributions are used to approximately portray the variations of

the properties of FG plates with porosities. The present theory is validated with the results available in the open literature. The numerical results estimated by the present theory are accurate in estimating the flexural response of perfect and porous FG plates. The influence of thickness ratio  $a/h$ , aspect ratio  $b/a$ , gradation index  $p$ , and porosity volume fraction of the flexural response of FG plates are studied. Also, the provided numerical results can be used to evaluate various plate theories and also to compare the results provided by other analytical methods and finite element methods. Based on the present work, it can be concluded that the present theory allows examining the flexural behavior of porous FG plates produced by sintering process.

## References

- [1] Zhu J., Lai Z., Yin Z., Jeon J., Lee S., 2001, Fabrication of ZrO<sub>2</sub>-NiCr functionally graded material by powder metallurgy, *Materials Chemistry and Physics*, doi: [https://doi.org/10.1016/S0254-0584\(00\)00355-2](https://doi.org/10.1016/S0254-0584(00)00355-2)
- [2] Mohammadi M., Ghayour M., Farajpour A., 2011, Analysis Of Free Vibration Sector Plate Based On Elastic Medium By Using New Version Of Differential Quadrature Method, *Journal Of Simulation And Analysis Of Novel Technologies In Mechanical Engineering (Journal Of Solid Mechanics In Engineering)* 3(2): 47-56.
- [3] Mohammadi M., Farajpour A., Goodarzi M., Mohammadi H., 2013, Temperature Effect on Vibration Analysis of Annular Graphene Sheet Embedded on Visco-Pasternak Foundation, *Journal of Solid Mechanics* 5(3): 305-323.
- [4] Safarabadi M., Mohammadi M., Farajpour A., Goodarzi M., 2015, Effect of Surface Energy on the Vibration Analysis of Rotating Nanobeam, *Journal of Solid Mechanics* 7(3): 299-311.
- [5] M. Baghani, M. Mohammadi, A. Farajpour, Dynamic and Stability Analysis of the Rotating Nanobeam in a Nonuniform Magnetic Field Considering the Surface Energy, *International Journal of Applied Mechanics*, doi:10.1142/S1758825116500484.
- [6] Goodarzi M., Mohammadi M. , Khooran M., Saadi F., 2016, Thermo-Mechanical Vibration Analysis of FG Circular and Annular Nanoplate Based on the Visco-Pasternak Foundation, *Journal of Solid Mechanics* 8(4): 788-805.
- [7] Şeref Doğuşcan Akbaş, 2017, Vibration and Static Analysis of Functionally Graded Porous Plates, *Journal of applied and computational mechanics*, doi: 10.22055/JACM.2017.21540.1107.
- [8] Zenkour A. M., 2018, A quasi-3D refined theory for functionally graded single-layered and sandwich plates with porosities, *Composite structures*, doi: <https://doi.org/10.1016/j.compstruct.2018.05.147>.
- [9] Nguyen Nam, Nguyen Hoang V., Lee X., Seungyhe, Nguyen-Xuan H, 2018, Geometrically nonlinear polygonal finite element analysis of functionally graded porous plates, *Advances in Engineering software*, doi: <https://doi.org/10.1016/j.advengsoft.2018.11.005>.
- [10] Li, Keyan, Di Wu, Xiaojun Chen, Jin Cheng, Zhenyu Liu, Wei Gao and Muyu Liu, 2018, Isogeometric Analysis of functionally graded porous plates reinforced by graphene platelets, *Composite structures*, doi: <https://doi.org/10.1016/j.compstruct.2018.07.059>.
- [11] Merdaci Slimane, 2018, Analysis of Bending of ceramic-metal functionally graded plates with porosities using of higher order shear theory, *Advanced Engineering Forum*, doi:10.4028/www.scientific.net/AEF.30.54.
- [12] Pinar Aydan DEMIRHAN, Vedat TASKIN, 2019, Bending and free vibration analysis of Levy-type porous functionally graded plate using state space approach, *Composite Part B: Engineering*, doi: <https://doi.org/10.1016/j.compositesb.2018.12.020>.
- [13] Semsi Coskun, Jinseok Kim, Houssam Toutanji, 2019, Bending, Free Vibration, and Buckling Analysis of Functionally Graded Porous Micro-Plates Using a General Third-Order Plate Theory, *Journal of composites science*, doi:10.3390/jcs3010015.
- [14] Jinseok Kim, Krzysztof KamilŻur, J.N Reddy, 2019, Bending, free vibration, and buckling of modified couples stress-based functionally graded porous micro-plates, *Composite structures* doi: <https://doi.org/10.1016/j.compstruct.2018.11.023>
- [15] Chen D., Yang J., Kitipornchai S, 2019, Buckling and bending analyses of a novel functionally graded porous plate using Chebyshev-Ritz method, *Archives of Civil and Mechanical Engineering*, doi: <https://doi.org/10.1016/j.acme.2018.09.004>.
- [16] Ahmed Amine Daikh , Zenkour A. M, 2019, Effect of porosity on the bending analysis of various functionally graded sandwich plates, *Materials research Express*, doi: <https://doi.org/10.1088/2053-1591/ab0971>.
- [17] Slimane Merdaci, Hakima Belghoul, 2019, High-order shear theory for static analysis of functionally graded plates with porosities, *C. R. Mécanique*, <https://doi.org/10.1016/j.crme.2019.01.001>.
- [18] Amir Farzam and Behrooz Hassani, 2019, Isogeometric analysis of in-plane functionally graded porous microplates using modified couple stress theory, *Aerospace Science and Technology*, doi: <https://doi.org/10.1016/j.ast.2019.05.012>.
- [19] Jing Zhao., Kwangnam Choe., Fei Xie, Ailun Wang, Cijun Shuai and Qingshan Wang, 2018, Three-dimensional exact solution for vibration analysis of thick functionally graded porous (FGP) rectangular plates with arbitrary boundary conditions, *Composites Part B: Engineering*, doi: <https://doi.org/10.1016/j.compositesb.2018.09.001>.
- [20] Zenkour A.M, 2007, Benchmark trigonometric and 3-D elasticity solutions for an exponentially graded thick rectangular plate, *Archieve of Applied Mechanics*, <https://doi.org/10.1007/s00419-006-0084-y>.
- [21] Mantari J.L., Guedes Soares C, 2013, A novel higher-order shear deformation theory with stretching effect for functionally graded plates, *Composites part B: Engineering*, <https://doi.org/10.1016/j.compositesb.2012.05.036>.